Multiphase patterns in periodically forced oscillatory systems

Christian Elphick
Centro de Fisica No Lineal y Sistemas Complejos de Santiago, Casilla 17122, Santiago, Chile

Aric Hagberg*
Theoretical Division and Center for Nonlinear Studies, MSB284, Los Alamos National Laboratory, Los Alamos, New Mexico 87545

Ehud Meron†
The Jacob Blaustein Institute for Desert Research and the Physics Department, Ben-Gurion University, Sede Boker Campus 84990, Israel

(Received 4 December 1998)

Periodic forcing of an oscillatory system produces frequency locking bands within which the system frequency is rationally related to the forcing frequency. We study extended oscillatory systems that respond to uniform periodic forcing at one quarter of the forcing frequency (the 4:1 resonance). These systems possess four coexisting stable states, corresponding to uniform oscillations with successive phase shifts of $\pi/2$. Using an amplitude equation approach near a Hopf bifurcation to uniform oscillations, we study front solutions connecting different phase states. These solutions divide into two groups: π fronts separating states with a phase shift of π and $\pi/2$ fronts separating states with a phase shift of $\pi/2$. We find a type of front instability where a stationary π front ''decomposes'' into a pair of traveling $\pi/2$ fronts as the forcing strength is decreased. The instability is degenerate for an amplitude equation with cubic nonlinearities. At the instability point a continuous family of pair solutions exists, consisting of $\pi/2$ fronts separated by distances ranging from zero to infinity. Quintic nonlinearities lift the degeneracy at the instability point but do not change the basic nature of the instability. We conjecture the existence of similar instabilities in higher $2n$:1 resonances ($n=3,4,\ldots$) where stationary π fronts decompose into n traveling π/n fronts. The instabilities designate transitions from stationary two-phase patterns to traveling $2n$-phase patterns. As an example, we demonstrate with a numerical solution the collapse of a four-phase spiral wave into a stationary two-phase pattern as the forcing strength within the 4:1 resonance is increased. [S1063-651X(99)06705-7]

PACS number(s): 05.45.−a, 82.40.Bj, 82.40.Ck, 47.20.Ma

I. INTRODUCTION

Periodic forcing of an oscillatory system produces a multiplicity of uniform stable phase states. The simplest situation arises within the 2:1 frequency locking band where the system oscillates at one half of the forcing frequency. In that case ''two-phase'' patterns appear, involving alternating domains that oscillate with a phase shift of π [1–3]. The boundaries between nearby domains, hereafter π fronts, may undergo a parity breaking bifurcation, rendering a stationary front unstable and giving rise to a pair of counterpropagating fronts [4]. This instability, the so-called nonequilibrium Ising-Bloch bifurcation (NIB) bifurcation, designates a transition from standing two-phase patterns to traveling two-phase patterns [5–7]. The instability is demonstrated in Fig. 1 as a gray-scale map in the space-time plane. Recent experiments on a photosensitive Belousov-Zhabotinsky (BZ) reaction, periodically illuminated, have also revealed a transition to labyrinthine patterns within the 2:1 band, suggesting the possible existence of a transverse instability of π fronts [8].

The situation becomes more complicated within the 4:1 band, which has four stable phase states shifted by $\pi/2$ with respect to one another [9]. In addition to π fronts, there also exist $\pi/2$ fronts separating oscillating domains with a phase shift of $\pi/2$. The multiplicity of front solutions increases with the order of the band. The 6:1 band has three types of fronts: π fronts, $2\pi/3$ fronts, and $\pi/3$ fronts. The 8:1 band has four types of fronts (π, $3\pi/4$, $\pi/2$, and $\pi/4$), and so on. In addition to adding new types of fronts, as the band order is increased the number of front solutions of a given type also increases.

In this paper we report on an instability of π fronts, occurring within the 4:1 band. Upon decreasing the forcing strength, a stationary π front loses stability and decomposes into a pair of traveling $\pi/2$ fronts. The instability is demonstrated in Fig. 2. The decomposition into a pair of traveling $\pi/2$ fronts is accompanied by the appearance of an intermediate (gray) domain whose phase of oscillation is shifted by $\pi/2$ with respect to the adjacent white and black domains. Like the NIB bifurcation, the π-front instability within the 4:1 band designates a transition from stationary patterns to traveling waves. The significant difference is that the two-phase stationary patterns give place to traveling *four-phase* patterns. This feature of the 4:1 resonance is related to a peculiar property of the π front instability to be discussed in Sec. III. The π front decomposition instability appears to exist in higher $2n$:1 bands as well. We analyze in detail the 4:1 resonance case and bring numerical evidence for the existence of this type of instability in the 6:1 and 8:1 resonances. A brief account of some of the results to be reported

*Electronic address: aric@lanl.gov
†Electronic address: ehud@bgumail.bgu.ac.il

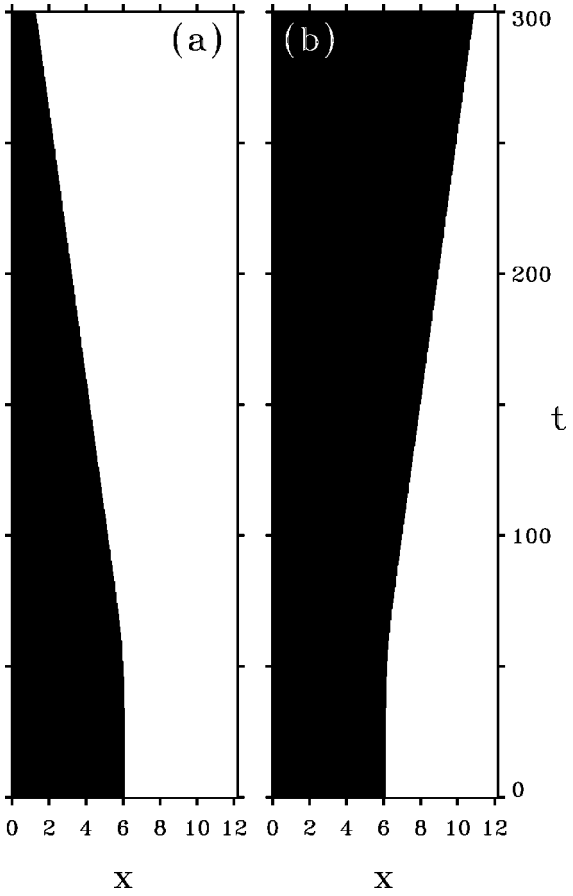

FIG. 1. The NIB bifurcation in the 2:1 resonance: space-time plots showing an unstable stationary π front (Ising) evolving into left (a) and right (b) traveling π fronts (Bloch) beyond the NIB bifurcation.

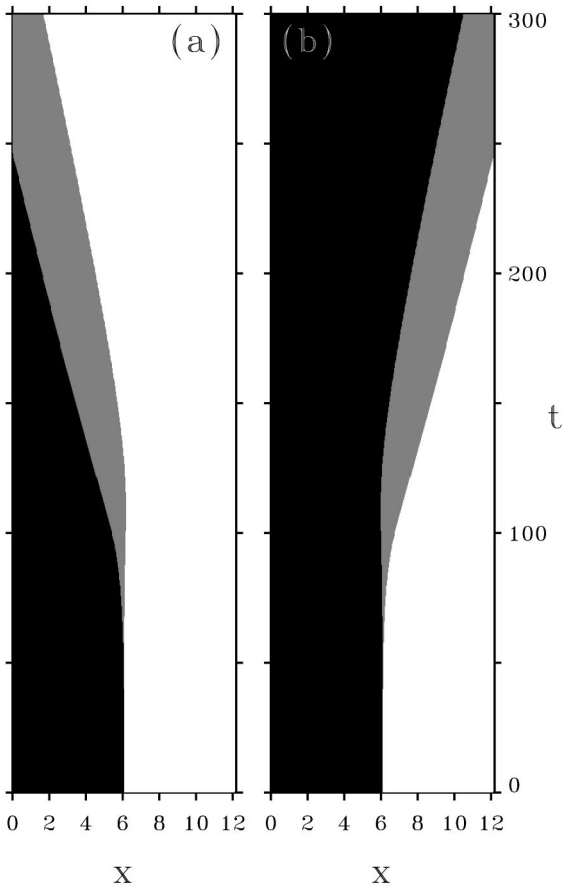

FIG. 2. The decomposition instability in the 4:1 resonance: Space-time plots [solutions of Eq. (1)] showing the decomposition of an unstable π front into a pair of $\pi/2$ fronts traveling to the left (a) or to the right (b). The pairs of $\pi/2$ fronts enclose grey colored domains whose oscillation phases are shifted by $\pi/2$ with respect to the black and white domains. Parameters in Eq. (1): $\mu=1.0$, $\nu=0.02$, $\gamma_4=0.3$.

here has appeared in Ref. [10].

We consider an extended system that is close to a Hopf bifurcation and externally forced with a frequency about four times larger than the Hopf frequency. The set of dynamical fields $\mathbf{u}$ describing the spatio-temporal state of the system (e.g., set of concentrations in the BZ reaction) can be written as $\mathbf{u}=\mathbf{u_0}A\exp(i\omega_f t/4)+\text{c.c.}+\ldots$, where $\mathbf{u_0}$ is constant, A is a slowly varying complex amplitude, ω_f is the forcing frequency, and the ellipses denote smaller contributions. The equation for the amplitude A can be written in the following standard form (after rescaling and shifting $\arg A$ by a constant phase) [11–14]:

$$A_\tau=(\mu+i\nu)A+(1+i\alpha)A_{zz}-(1-i\beta)|A|^2A+\gamma_4A^{*3}, \tag{1}$$

where the subscripts τ and z denote partial derivatives with respect to time and space, and all the parameters are real. The proximity to the Hopf bifurcation implies $\mu\ll 1$. We will also be using the following form of Eq. (1) obtained by rescaling time, space, and amplitude as $t=\mu\tau$, $x=\sqrt{\mu/2}z$, and $B=A/\sqrt{\mu}$:

$$B_t=(1+i\nu_0)B+\tfrac{1}{2}(1+i\alpha)B_{xx}-(1-i\beta)|B|^2B+\gamma_4B^{*3}, \tag{2}$$

where $\nu_0=\nu/\mu$.

II. FRONT SOLUTIONS

First we study the gradient version of Eq. (2), which is obtained by setting $\nu_0=\alpha=\beta=0$:

$$B_t=B+\tfrac{1}{2}B_{xx}-|B|^2B+\gamma_4B^{*3}. \tag{3}$$

Equation (3) has four stable phase states for $0<\gamma_4<1$ shown by solid circles in Fig. 3: $B_{\pm 1}=\pm\lambda$ and $B_{\pm i}=\pm i\lambda$, where $\lambda=1/\sqrt{1-\gamma_4}$. Front solutions connecting pairs of these states divide into two groups, π fronts and $\pi/2$ fronts. The π fronts, shown in Fig. 3 as solid lines, are given by

$$B_{-1\to+1}=B_{+1}\tanh x,$$

$$B_{-i\to+i}=B_{+i}\tanh x. \tag{4}$$

The $\pi/2$ fronts are shown in Fig. 3 by the dashed curves. For the particular parameter value $\gamma_4=1/3$ they have the simple forms

$$B_{+1\to+i}=\frac{1}{2}\sqrt{\frac{3}{2}}\,[1+i-(1-i)\tanh x],$$

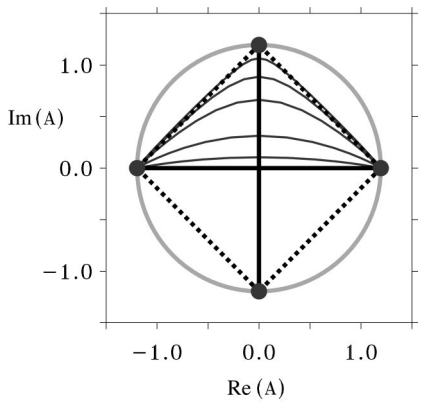

FIG. 3. Phase portrait in the complex plane of solutions to Eq. (3). The dots represent the four spatially uniform phase-locked solutions. The solid lines are the π-front solutions and the dashed lines are the $\pi/2$ fronts. The thin lines in the circle are the phase portrait showing the collapse of a π front into two $\pi/2$ fronts.

$$B_{-i\to+1}=\frac{1}{2}\sqrt{\frac{3}{2}}\,[1-i+(1+i)\tanh x],$$

$$B_{+i\to-1}=-B_{-i\to+1},$$

$$B_{-1\to-i}=-B_{+1\to+i}. \tag{5}$$

Additional front solutions follow from the invariance of Eq. (3) under reflection, $x\to -x$. For example, the symmetric counterparts of $B_{+i\to+1}(x)$ and $B_{+1\to-i}(x)$ are $B_{+1\to+i}(x)=B_{+i\to+1}(-x)$ and $B_{-i\to+1}(x)=B_{+1\to-i}(-x)$.

Consider now the nongradient system (2). The main effect of the nongradient terms is to make the $\pi/2$ fronts traveling. The nongradient terms have no effect on the π fronts, which remain stationary. To see this we assume a traveling solution $B(x-ct)$ of Eq. (2) and project this equation on the translational mode B'. For π fronts we obtain

$$c\langle B_0'^2\rangle=0, \quad B_0(z)=\lambda\tanh z, \tag{6}$$

implying $c=0$ (the brackets denote integration over the whole line). For $\pi/2$ fronts with $\gamma_4=1/3$, we find

$$|c|=\frac{\lambda}{\langle B_0'^2\rangle}[(\nu_0+\tfrac{1}{2}\lambda^2\beta)\langle B_0'\rangle+\tfrac{1}{2}\beta\langle B_0^2B_0'\rangle]=\tfrac{3}{2}(\nu_0+\beta), \tag{7}$$

where $\lambda=\sqrt{3/2}$. A perturbation analysis around $\gamma_4=1/3$ shows that expression (7) for the speed remains valid for small deviations of γ_4 from 1/3.

III. A π-FRONT INSTABILITY

The π fronts (4) are similar to the Ising front in the 2:1 band but as we will see shortly the instability they undergo is not a pitchfork bifurcation like the NIB. It is rather a degenerate instability leading to asymptotic solutions that are not smooth continuations of the unstable stationary π fronts in a sense to be made clear in the following. A stability analysis of the π fronts indicates that they lose stability at $\gamma_4=1/3$. To analyze the instability, we study Eq. (2) near that critical value.

A. Gradient system

We begin with the gradient version (3). Introducing the new variables,

$$U=\mathrm{Re}(B)+\mathrm{Im}(B) \quad V=\mathrm{Re}(B)-\mathrm{Im}(B), \tag{8}$$

we rewrite Eq. (3) as

$$U_t=U+\frac{1}{2}U_{xx}-\frac{2}{3}U^3-\frac{d}{2}(U^2-3V^2)U, \tag{9a}$$

$$V_t=V+\frac{1}{2}V_{xx}-\frac{2}{3}V^3-\frac{d}{2}(V^2-3U^2)V, \tag{9b}$$

where

$$d=\gamma_4-1/3.$$

At the instability point, $\gamma_4=1/3$, the two equations decouple (since $d=0$) and admit solutions of the form

$$U=\sigma_1B_0(x-x_1),$$

$$V=\sigma_2B_0(x-x_2), \tag{10}$$

where $B_0(x)=\sqrt{(3/2)}\tanh x$, $\sigma_{1,2}=\pm 1$, and x_1 and x_2 are arbitrary constants. An intuitive understanding of this family of solutions can be obtained by expressing these solutions back in terms of the complex amplitude B. For $\sigma_1=-\sigma_2=1$, for example, the solution (10) is equivalent to

$$B(x;x_1,x_2)=B_{-i\to+1}(x-x_1)+B_{+1\to+i}(x-x_2)-\lambda.$$

When $|x_2-x_1|\to\infty$ this form approaches a pair of isolated $\pi/2$ fronts:

$$B\approx B_{-i\to+1}(x-x_1), \quad x\approx x_1$$

and

$$B\approx B_{+1\to+i}(x-x_2), \quad x\approx x_2.$$

When $x_2-x_1=0$ it reduces to the π front $B_{-i\to+i}$. Defining a ''center-of-mass'' coordinate ζ and an order parameter χ by

$$\zeta=\tfrac{1}{2}(x_1+x_2), \quad \chi=\tfrac{1}{2}(x_2-x_1),$$

the one-parameter family of solutions, $\{\tilde{B}(x;\zeta,\chi)|\chi\in R\}$, where $\tilde{B}(x;\zeta,\chi)=B(x;x_1,x_2)$, represents $\pi/2$-front pairs with distances 2χ ranging from zero to infinity.

For $|\gamma_4-1/3|=|d|\ll 1$, the weak coupling between Eqs. (9a) and (9b) induces slow drift along the solution family $B(x;x_1,x_2)$. We now write a pair solution as

$$U=\sigma_1B_0[x-x_1(t)]+u,$$

$$V=\sigma_2B_0[x-x_2(t)]+v, \tag{11}$$

where u and v are corrections of order d. Inserting these forms in Eqs. (9) we obtain,

$$\mathcal{H}_1 u = \sigma_1 \dot{x}_1 B_0'(x-x_1) - \tfrac{1}{2} d\sigma_1 [B_0^2(x-x_1) - 3B_0^2(x-x_2)] B_0(x-x_1), \tag{12}$$

$$\mathcal{H}_2 v = \sigma_2 \dot{x}_2 B_0'(x-x_2) - \tfrac{1}{2} d\sigma_2 [B_0^2(x-x_2) - 3B_0^2(x-x_1)] B_0(x-x_2), \tag{13}$$

where $\mathcal{H}_{1,2} = -1 - \frac{1}{2}\partial^2/\partial x^2 + 2B_0^2(x-x_{1,2})$. Projecting the right-hand side of Eq. (12) onto $B_0'(x-x_1)$, the zero eigenmode of $\mathcal{H}_1^\dagger = \mathcal{H}_1$, and setting to zero we obtain,

$$\dot{x}_1 = -\frac{27}{16} d \int_{-\infty}^{\infty} dx \tanh(x-x_1)\operatorname{sech}^2(x-x_1)\tanh^2(x-x_2). \tag{14}$$

A similar solvability condition for Eq. (13) leads to

$$\dot{x}_2 = -\frac{27}{16} d \int_{-\infty}^{\infty} dx \tanh(x-x_2)\operatorname{sech}^2(x-x_2)\tanh^2(x-x_1). \tag{15}$$

Expressing these equations in terms of ζ and χ, we find

$$\dot{\zeta} = 0, \tag{16}$$

$$\dot{\chi} = -\tfrac{27}{16} d J(\chi), \tag{17}$$

where

$$J(\chi) = \int_{-\infty}^{\infty} dz \tanh z \operatorname{sech}^2 z \tanh^2(z+2\chi). \tag{18}$$

Evaluation of the integral in Eq. (18) yields

$$J(\chi) = I(a) = 6(a^{-1} - a^{-3}) + (1-3a^{-2})G(a),$$

$$G(a) = (1-a^{-2})\ln\left(\frac{1+a}{1-a}\right),$$

where $a = \tanh 2\chi$. Note that Eqs. (16) and (17) are valid to *all* orders in χ and to linear order around $\gamma_4 = 1/3$.

The equation for the order parameter (17) can be written in the gradient form

$$\dot{\chi} = -\frac{dV}{d\chi}, \quad V = \frac{27}{16} d \int^{\chi} J(z) dz. \tag{19}$$

Figure 4 shows the potential $V(\chi)$ for $d>0$ ($\gamma_4 > 1/3$) and $d<0$. There is only one extremum point $\chi = 0$ of V. For $d>0$ it is a minimum and χ converges to zero. Pairs of $\pi/2$ fronts with arbitrary initial separation $x_2 - x_1$ attract one another and eventually collapse to a single π front ($x_1 = x_2$ or $\chi = 0$). In practice, the collapse process is noticeable only for relatively small separations. For $d<0$ the extremum point $\chi = 0$ is a maximum and χ diverges to $\pm\infty$. A π front decomposes into a pair of $\pi/2$ fronts, which repel one another. This process is shown in Fig. 2 for the nongradient system (1). In the gradient case both π and $\pi/2$ fronts are stationary (in the absence of interactions). Since the potential $V(\chi)$ becomes practically flat at finite χ values, the pair of $\pi/2$ fronts do not seem to depart from one another at long times.

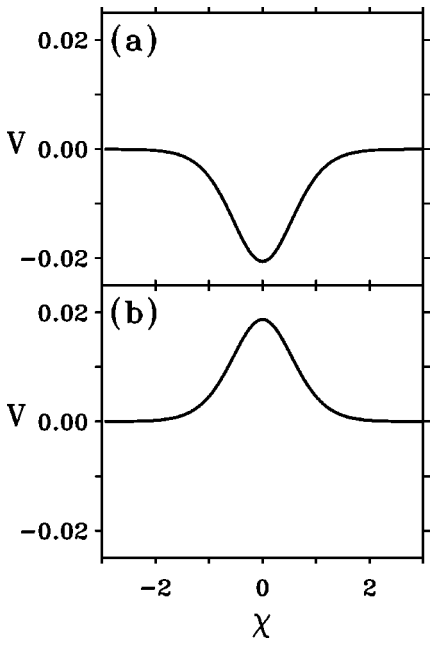

FIG. 4. The potential $V(\chi)$. (a) For $d>0$ the extremum at $\chi = 0$ is a minimum and χ converges to 0. (b) For $d<0$ the extremum is a maximum and χ diverges to $\pm\infty$.

Figure 3 shows the decomposition process of a π front in the complex B plane. Starting with the $B_{-1\to+1}$ π front, represented by the thick solid phase portrait, the time evolution (thin solid phase portraits) is toward the fixed point B_{+i} and the dashed phase portraits representing the pair of $\pi/2$ fronts $B_{+1\to+i}$ and $B_{+i\to-1}$. Because of the parity symmetry $\chi \to -\chi$, an appropriate perturbation of the initial $B_{-1\to+1}$ π front could have led the dynamics toward the pair $B_{+1\to-i}$ and $B_{-i\to-1}$. Notice that for $d=0$, $\dot{\zeta}=0$, $\dot{\chi}=0$, and we recover the two-parameter family of pair solutions $B(x;\zeta,\chi)$ with arbitrary ζ and χ. This degeneracy of solutions at $d=0$ is lifted by higher-order terms in the amplitude equation (1) as will be discussed in Sec. III C below.

B. Nongradient system

The results described above can easily be extended to the nongradient system (2) for small α, β, and ν_0. The equations for U and V are

$$U_t = U + \frac{1}{2}U_{xx} - \frac{2}{3}U^3 - \frac{d}{2}(U^2-3V^2)U + \nu_0 V + \frac{\alpha}{2}V_{xx} + \frac{\beta}{2}(U^2+V^2)V,$$

$$V_t = V + \frac{1}{2}V_{xx} - \frac{2}{3}V^3 - \frac{d}{2}(V^2-3U^2)V - \nu_0 U - \frac{\alpha}{2}U_{xx} - \frac{\beta}{2}(U^2+V^2)U. \tag{20}$$

Assuming d, α, β, and ν_0 are of the same order of magnitude we write a solution in the form (11), insert in Eqs. (20), and obtain,

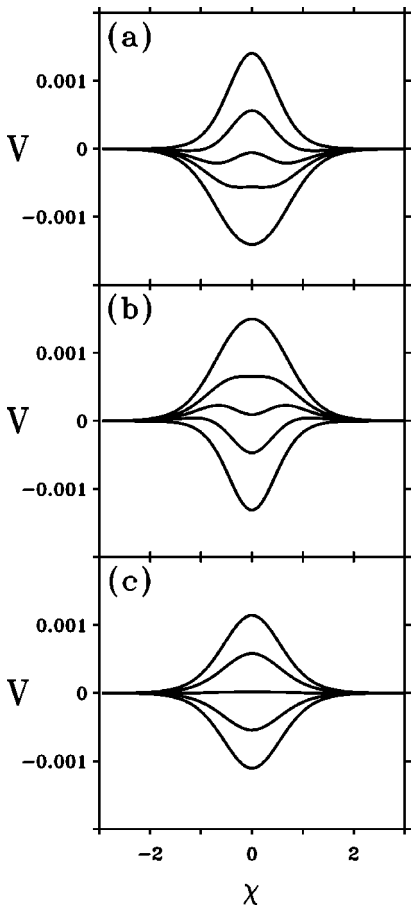

FIG. 5. The effects of the higher-order term $\delta|B|^2B_{xx}$ on the decomposition instability within the 4:1 resonance. The potential (27) deforms from a single well to a single barrier as γ_4 is decreased past γ_{4c}. In the intermediate range two scenarios are possible: (a) For $\delta>0$, the $\chi=0$ solution loses stability in a pitchfork bifurcation at γ_{4c} to a pair of solutions that move to $\pm\infty$. Parameters: $\delta=1.0$, $\mu=0.01$, $\gamma_4=0.339,0.337,0.336,0.335,0.333$. (b) For $\delta<0$, the $\chi=0$ solution remains stable while the $\chi=\pm\infty$ solutions acquire stability and lose stability only below γ_{4c}. Parameters: $|\delta|=1.0$, $\mu=0.01$, $\gamma_4=0.334,0.332,0.331,0.330,0.328$. In both scenarios the deformations from a single well to a single barrier occur within a small range of γ_4 of order $\mu\ll1$. For comparison, an equivalent figure for the degenerate case ($\delta=0$) is shown in (c). The only intermediate form between a single well and a single barrier is a flat potential, $V=0$, ocurring at $\gamma=1/3$.

$$\mathcal{H}_1 u=\sigma_1\dot{x}_1B_0'(x-x_1)-\tfrac{1}{2}d\sigma_1[B_0^2(x-x_1)-3B_0^2(x-x_2)]B_0(x-x_1)+\nu_0\sigma_2B_0(x-x_2)+\tfrac{1}{2}\alpha\sigma_2B_0''(x-x_2)+\tfrac{1}{2}\beta\sigma_2[B_0^2(x-x_1)+B_0^2(x-x_2)]B_0(x-x_2), \tag{21}$$

$$\mathcal{H}_2 v=\sigma_2\dot{x}_2B_0'(x-x_2)-\tfrac{1}{2}d\sigma_2[B_0^2(x-x_2)-3B_0^2(x-x_1)]B_0(x-x_2)-\nu_0\sigma_1B_0(x-x_1)-\tfrac{1}{2}\alpha\sigma_1B_0''(x-x_1)-\tfrac{1}{2}\beta\sigma_1[B_0^2(x-x_1)+B_0^2(x-x_2)]B_0(x-x_1). \tag{22}$$

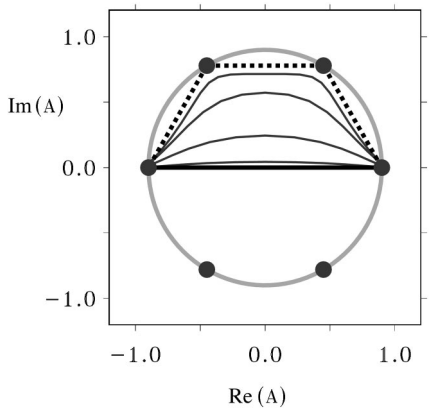

FIG. 6. Decomposition of a π front into three $\pi/3$ fronts in the 6:1 resonance band. Parameters in Eq. (28): $\gamma_6=0.9$, $\mu_4=-1.0$, $\mu_6=-1.0$. All other parameters are zero.

Solvability conditions lead to equations for χ and ζ. The equation for χ remains unchanged. That is, Eq. (17) is valid for the nongradient equation (2) as well. The equation for ζ becomes

$$\sigma_1\sigma_2\dot{\zeta}=\nu_0F_\nu(\chi)+\alpha F_\alpha(\chi)+\beta F_\beta(\chi), \tag{23}$$

where

$$F_\nu=-\tfrac{3}{4}G(a)-\tfrac{3}{2}a^{-1},$$

$$F_\alpha=\tfrac{3}{4}I(a),$$

$$F_\beta=3a^{-1}(1-\tfrac{3}{2}a^{-2})-\tfrac{9}{4}a^{-2}G(a).$$

Notice that F_ν, F_α, and F_β are odd functions of χ and do not vanish when $d=0$. When $|\chi|\to\infty$, the right-hand side of Eq. (23) converges to $\frac{3}{2}(\nu_0+\beta)$, the speed of a $\pi/2$-front solution of Eq. (2). The odd symmetries of F_ν, F_α, and F_β imply that the $\chi=0$ solution (representing a π front) remains stationary ($\dot{\zeta}=0$) in the nongradient case as well, and that the two pairs of $\pi/2$ fronts $\chi=\pm\infty$ propagate in opposite directions.

C. The effect of higher-order terms

According to Eq. (17) the asymptotic solutions just below $\gamma_4=1/3$, the $\pi/2$-front pairs as $|\chi|\to\infty$, are not smooth continuations of the stationary π front at $\gamma_4=1/3$ (the $\chi=0$ solution). This abrupt nature of the instability is related to a degeneracy of solutions at $\gamma_4=1/3$. At this parameter value a whole family of solutions exists describing $\pi/2$-front pairs with distances $|x_2-x_1|=2|\chi|$ ranging from zero to infinity. In the nongradient case these pair solutions propagate at speeds given by Eq. (23). The degeneracy of solutions is lifted by higher-order terms in Eq. (2).

Consider the gradient version of the amplitude equation,

$$B_t=B+\tfrac{1}{2}B_{xx}-|B|^2B+\gamma_4B^{*3}+\mu H(B,B^*;\partial_x), \tag{24}$$

where $H(B,B^*;\partial_x)$ includes higher-order terms like $|B|^4B$, $|B|^2B_{xx}$, etc. The factor μ reflects the fact that fifth-order terms in the amplitude equation are smaller by a factor $\mu\ll1$ than the lower-order terms. The effect of these terms is

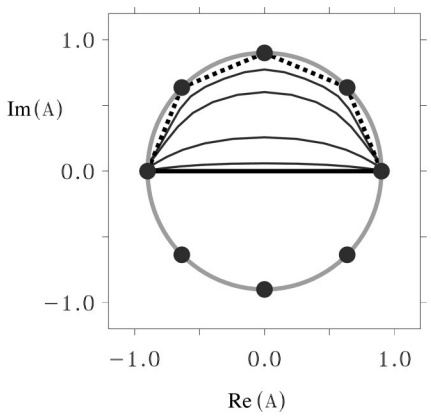

FIG. 7. Decomposition of a π front into four $\pi/4$ fronts in the 8:1 resonance band. Parameters in Eq. (28): $\gamma_8=0.75$, $\mu_4=-0.5$, $\mu_6=-0.5$, $\mu_8=-1.0$. All other parameters are zero.

generally weak, but becomes important near $\gamma_4=1/3$. Consider, for example, the effect of the term $\delta|B|^2B_{xx}$. Equations (9) include now the contributions

$$\tfrac{1}{2}\mu\delta(U^2+V^2)U_{xx} \quad \text{and} \quad \tfrac{1}{2}\mu\delta(U^2+V^2)V_{xx},$$

respectively. The corresponding contributions to Eqs. (12) and (13) are

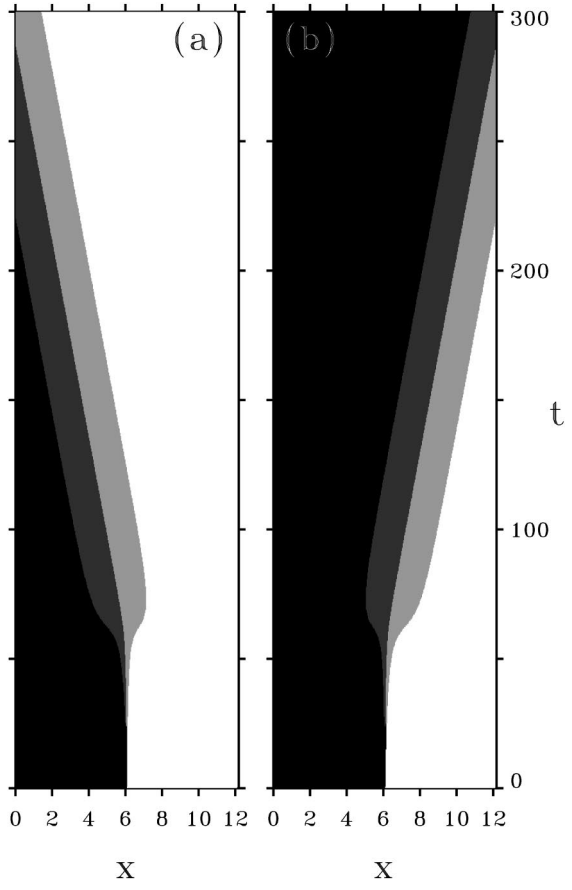

FIG. 8. Decomposition of a π front into three $\pi/3$ fronts in the 6:1 resonance band. The figures show space-time plots of numerical solutions of Eq. (28) with parameters $\gamma_6=0.9$, $\mu_4=-1.0$, $\mu_6=-1.0$, $\nu_0=0.1$. All other parameters are zero.

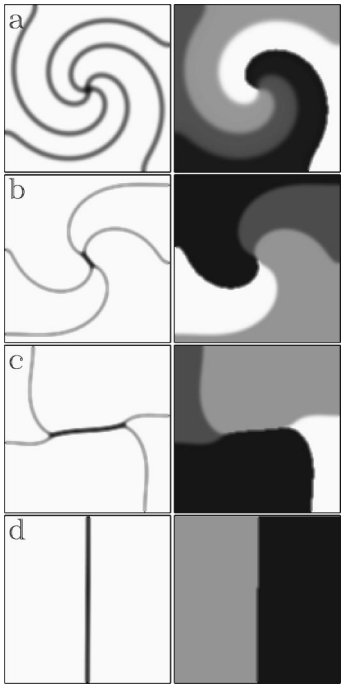

FIG. 9. Numerical solution of a two-dimensional version of Eq. (2) showing the collapse of a rotating four-phase spiral wave into a stationary two-phase pattern. The left column is $|A|$ and the right column arg(A) in the x-y plane. (a) The initial four-phase spiral wave (computed with $\gamma_4<1/3$). (b) The spiral core, a four-point vertex, splits into two three-point vertices connected by a π front. (c) A two-phase pattern develops as the three-point vertices further separate. (d) The final stationary two-phase pattern. Parameters: $\gamma_4=0.6$, $\nu_0=0.1$, $\alpha=\beta=0$, $x=[0,64]$, $y=[0,64]$.

$$\tfrac{1}{2}\mu\delta\sigma_1[B_0^2(x-x_1)+B_0^2(x-x_2)]B_0''(x-x_1)$$

and

$$\tfrac{1}{2}\mu\delta\sigma_2[B_0^2(x-x_1)+B_0^2(x-x_2)]B_0''(x-x_2).$$

The equation for the order parameter will now read

$$\dot{\chi}=-\tfrac{27}{16}dJ(\chi)+\tfrac{9}{8}\delta\mu K(\chi), \tag{25}$$

where

$$K(\chi)=\int_{-\infty}^{\infty}dz\,\tanh z\,\mathrm{sech}^4 z\,\tanh^2(z+2\chi). \tag{26}$$

The integral (26) is elementary but the expression is lengthy and we do not display it here. The second term on the right-hand side of Eq. (25), whose origin is the fifth-order term $|B|^2B_{xx}$, cannot be neglected in a μ neighborhood of $\gamma_4=1/3$. Depending on the sign of δ two scenarios are possible as γ_4 is decreased. In both cases the $\chi=0$ (π-front) solution is destabilized at $\gamma_{4c}=1/3+8\mu\delta/21$. When $\delta>0$ the $\chi=0$ solution is destabilized to a new pair of solutions $\chi_\pm$ in a pitchfork bifurcation. For $|\chi|\ll 1$ the solutions assume the approximate values, $\chi_\pm\approx\pm\sqrt{21/4}\sqrt{1-d/d_c}$, where $d_c=\gamma_{4c}-1/3$. When γ_4 is further decreased, the two stable solutions $\chi_\pm$ move to $\pm\infty$ on a γ_4 range of order μ. When $\delta<0$ bistability of the $\chi=0$ solution and the $\chi=\pm\infty$ solutions first develop. As γ_4 is further decreased the $\chi=0$ so-

lution becomes metastable until it completely loses its stability at γ_{4c}. Figure 5 shows the potential

$$V=\frac{9}{8}\int^{\chi}\left[\frac{3}{2}dJ(z)-\delta\mu K(z)\right]dz, \tag{27}$$

associated with Eq. (25) for both scenarios.

The two scenarios are related by the symmetry $d\to -d$, $\delta\to -\delta$, $t\to -t$, of Eq. (25). The first scenario ($\delta>0$) amounts to a pitchfork bifurcation from a stable $\chi=0$ solution to a pair of stable $\chi_{\pm}$ solutions that move to infinity as γ_4 is decreased. The second scenario ($\delta<0$) amounts to a backward pitchfork bifurcation from an unstable $\chi=0$ solution to a pair of unstable $\chi_{\pm}$ solutions that move to infinity as γ_4 is increased.

The higher-order term $|B|^2B_{xx}$, and similarly other high-order terms, lift the degeneracy of the lower-order system (3) at $\gamma_4=1/3$. For $\delta>0$ and in a small γ_4 range of order μ near 1/3, the instability becomes similar to the NIB bifurcation in the 2:1 resonance. But apart from the behavior in this small parameter range, the overall behavior does not change: a π front decomposes into a pair of $\pi/2$ fronts as γ_4 is decreased.

IV. π-FRONT INSTABILITIES IN HIGHER RESONANCES

We have found numerical evidence for the existence of similar π-front instabilities within the 6:1 and 8:1 bands. These findings suggest the following generalization: within the $2n$:1 band ($n>1$) a π front may lose stability by decomposing into n π/n fronts. Consider the equation

$$B_t=\tfrac{1}{2}B_{xx}+(1+i\nu_0)B+\mu_4|B|^2B+\mu_6|B|^4B+\mu_8|B|^6B+\gamma_4B^{*3}+\gamma_6B^{*5}+\gamma_8B^{*7}. \tag{28}$$

The normal form equation up to seventh order contains many more terms. Our purpose here, however, is just to demonstrate the π-front instability for *some* parameter values pertaining to the 6:1 and 8:1 bands. Figure 6 shows the decomposition in the complex B plane of a π front within the 6:1 band into three $\pi/3$ fronts. Figure 7 shows the decomposition of a π front within the 8:1 band into four $\pi/4$ fronts.

Figure 8 shows a space-time plot of the decomposition instability within the 6:1 band. The initial unstable π front decomposes into three $\pi/3$ fronts, traveling to the left or to the right depending on initial conditions. Along with this process two intermediate phase states appear between the original white and black phases.

V. IMPLICATIONS ON PATTERN FORMATION

The π-front instability in the 4:1 band has a pronounced effect on patterns. Despite the coexistence of four uniform phase states and the stability of $\pi/2$ fronts, asymptotic four-phase patterns appear only below the π-front instability point $\gamma_4=1/3$. The reason is the attractive interactions between $\pi/2$ fronts when $\gamma_4>1/3$ and the collapse into π fronts. Thus, for $\gamma_4>1/3$ two-phase patterns prevail. These patterns form standing waves since π fronts are stationary. For $\gamma_4<1/3$ the interaction between $\pi/2$ fronts is repulsive and four-phase patterns prevail. These patterns travel since $\pi/2$ fronts propagate.

Figure 9(a) shows a stably rotating four-phase spiral wave for $\gamma_4<1/3$. Figures 9(b), 9(c), and 9(d) show the collapse of this spiral wave into a stationary two-phase pattern as γ_4 is increased past 1/3. The collapse begins at the spiral core where the $\pi/2$-front interactions are the strongest. As pairs of $\pi/2$ fronts attract and collapse into π fronts, the core splits into two vertices that propagate away from each other leaving behind a two-phase pattern.

ACKNOWLEDGMENTS

The authors thank J. Guckenheimer and B. Krauskopf for helpful discussions. This study was supported in part by Grant No. 95-00112 from the U.S.-Israel Binational Science Foundation (BSF).

[1] D. Walgraef, *Spatio-Temporal Pattern Formation* (Springer-Verlag, New York, 1997).
[2] P. Coullet and K. Emilsson, Physica D **61**, 119 (1992).
[3] B. A. Malomed and A. A. Nepomnyashcy, Europhys. Lett. **27**, 649 (1994).
[4] P. Coullet, J. Lega, B. Houchmanzadeh, and J. Lajzerowicz, Phys. Rev. Lett. **65**, 1352 (1990).
[5] A. Hagberg and E. Meron, Nonlinearity **7**, 805 (1994).
[6] M. Bode, A. Reuter, R. Schmeling, and H.-G. Purwins, Phys. Lett. A **185**, 70 (1994).
[7] C. Elphick, A. Hagberg, E. Meron, and B. Malomed, Phys. Lett. A **230**, 33 (1997).
[8] V. Petrov, Q. Ouyang, and H. L. Swinney, Nature (London) **388**, 655 (1997).
[9] B. Krauskopf, Ph.D. thesis, Rijksuniversiteit Groningen, 1995.
[10] C. Elphick, A. Hagberg, and E. Meron, Phys. Rev. Lett. **80**, 5007 (1998).
[11] A. C. Newell, in *Lectures in Applied Mathematics* (American Mathematical Society, Providence, RI, 1974), Vol. 15, p. 157.
[12] J. M. Gambaudo, J. Diff. Eqns. **57**, 172 (1985).
[13] C. Elphick, G. Iooss, and E. Tirapegui, Phys. Lett. A **120**, 459 (1987).
[14] M. C. Cross and P. C. Hohenberg, Rev. Mod. Phys. **65**, 851 (1993).